Chemical Physics Letters xxx (2010) xxx–xxx

Contents lists available at ScienceDirect

Chemical Physics Letters

journal homepage: www.elsevier.com/locate/cplett

Theoretical study of the molecular properties and the formation kinetics of the $FS(O_2)OCO$ radical

M.E. Tucceri, L.B. Bracco, C.J. Cobos *

Instituto de Investigaciones Fisicoquímicas Teóricas y Aplicadas (INIFTA), Departamento de Química, Facultad de Ciencias Exactas, Universidad Nacional de La Plata, CCT La Plata-CONICET, Casilla de Correo 16, Sucursal 4, 1900 La Plata, Argentina

ARTICLE INFO

Article history:
Received 12 December 2009
In final form 12 March 2010
Available online xxxx

ABSTRACT

Molecular and kinetics properties of the $FS(O_2)OCO$ radical have been studied. Equilibrium structure, harmonic vibrational frequencies, conformational mobilities, enthalpy of formation of this radical and the energetic of the reaction $FSO_3 + CO \rightarrow FS(O_2)OCO$ have been investigated at different levels of the density functional theory and of the Gaussian composite models. The standard enthalpy of formation for $FS(O_2)OCO$ is predicted to be $\Delta H_{f,298} = -155.0$ kcal mol^{-1}. In very good agreement with reported experimental values, a rate coefficient at 296 K of 3.6×10^{-17} cm^3 molecule^{-1} s^{-1} and an activation energy of 7.6 kcal mol^{-1} have been calculated.

1. Introduction

Kinetic studies of fluorosulfate radical FSO_3 reactions have received a considerable deal of attention. Early steady-state mechanistic studies [1–3] were more recently followed by theoretical and real-time resolved investigations [4–10]. From another point of view, the interest for the spectroscopy of this radical has been recently renewed. In fact, the first systematic spectroscopic studies of the vibrational, rotational and electronic spectra of FSO_3 [11] have been very recently improved by more detailed and sophisticated studies [12,13]. In addition, ozone depleting catalytic cycles with the participation of FSO, FSO_2 and FSO_3 radicals might be operating in rich SO_2 industrialized regions, active volcanic areas and in the marine biosphere [14].

A number of recombination reactions of the FSO_3 radical with F [4], FSO_3 [5,7], Cl [6], FC(O)O [8,9], CO [8,9] and FSO_2 [10] have been experimentally and theoretically investigated. In addition, indirect experimental data for the reaction (1) have been reported in Refs. [2,3].

$$FSO_3 + CO \rightarrow FS(O_2)OCO \quad (1)$$

Continuing with these studies, a theoretical analysis of both, the $FS(O_2)OCO$ radical properties and its reaction kinetics is presented here.

The activated process (1) has been postulated to explain the mechanism of the thermal reaction between the peroxide $FS(O_2)OO(O_2)SF$ and CO over the 263–298 K temperature range [2]. Under these conditions, the established $FS(O_2)OO(O_2)SF \Leftrightarrow 2FSO_3$ equilibrium [1,5] provides FSO_3 radicals, being the reaction products exclusively $FS(O_2)O(O_2)SF$ and CO_2. The analysis of the reaction mechanism leads to an activation energy for reaction (1) of (7 ± 1) kcal mol^{-1}. In the presence of O_2, the catalytic oxidation of CO is operative and the only reaction product is CO_2 [3]. More recently, reaction (1) has been directly observed in laser flash photolysis studies of $FS(O_2)OF$ in the presence of CO and O_2 at 296 K [8,9]. Besides of the determination of the rate coefficient for the formation of the novel peroxide $FC(O)OO(O_2)SF$ from FSO_3 and FC(O)O radicals, a limiting high pressure rate coefficient for reaction (1) of $k_{\infty,1} = (4.3 \pm 0.9) \times 10^{-17}$ cm^3 molecule^{-1} s^{-1} was measured. In qualitative agreement with the experiments of Ref. [2], this small value suggests the presence of an activated process. The potential importance of $FS(O_2)OCO$ radical in atmospheric chemistry is mainly related to the relevance of the afore-mentioned ozone destruction cycle induced by FSO_x ($x = 1$–3) radicals [14].

This Letter is concerned with a quantum-chemical and kinetic study of $FS(O_2)OCO$ radical. In particular, reliable molecular structures, conformational mobilities, harmonic vibrational frequencies, the enthalpy of formation and the rate coefficient for reaction (1) have been calculated by using recent formulations of the density functional theory (DFT), high-level composite model chemistries and transition state theory.

2. Computational methods

The traditional hybrid functional B3LYP [15,16] and the set of recent formulations B98 [17], B97-2 [18,19], O3LYP [20], X3LYP [21] and BMK [22], as implemented in the GAUSSIAN 03 program package, were employed [23]. The large 6-311+G(3df) triple split valence basis set was employed in the calculations. For hydrogen containing compounds, diffuse and p and d functions were

* Corresponding author. Fax: +54 221 4254642.
E-mail address: cobos@inifta.unlp.edu.ar (C.J. Cobos).

0009-2614/$ - see front matter © 2010 Elsevier B.V. All rights reserved.
doi:10.1016/j.cplett.2010.03.036

included on these atoms, 6-311++G(3df,3pd). The used diffuse and polarization functions allow for radial and angular flexibility of the basis set. Geometry optimisations without symmetry constraints were carried out using analytical gradient methods. At the calculated equilibrium structures, the harmonic vibrational frequencies were then derived via analytical second derivative methods. The synchronous transit-guided quasi-Newton (STQN) methods were employed for locating transition structures. At a higher level of theory, the *ab initio* Gaussian-3 model chemistry [24] and the more accurate recent implementation G4 were employed [25]. The B3LYP/6-311++G(3df,3pd) instead of the B3LYP/6-31G(d) level was used for the determination of the geometries and the vibrational frequencies in the Gaussian-3 models. In addition, to reduce systematic errors arisen in the Gaussian-3 treatment, bond additivity corrections (BAC) to correct efficiently for atomic, molecular and bondwise deficiencies were carried out [26]. The DFT computed geometrical values were compared with those derived at the high correlated coupled cluster singles and doubles approach CCSD/6-311G(d).

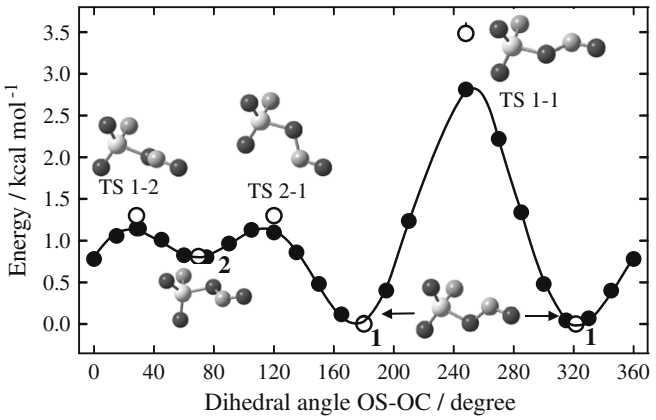

Fig. 2. Potential energy barriers for internal rotation around the OS–OC bond in $FS(O_2)OCO$. (●) B3LYP/6-311+G(3df); (○) G3(MP2)//B3LYP/6-311+G(3df); (—) calculated with Eq. (2) using the coefficients (in kcal mol^{-1}): $a_0 = 1.0004$, $b_1 = -0.1507$, $b_2 = -0.5826$, $b_3 = 0.5385$, $c_1 = -0.3640$, $c_2 = 0.5401$ and $c_3 = 0.2638$.

3. Results and discussion

3.1. Torsional barriers

The $FS(O_2)OCO$ radical presents internal rotations around the SO–CO and OS–OC bonds. In order to analyse the nature of these hindered motions, they were, for simplicity, separately analysed. For this, the total energy as a function of the dihedral angles was calculated by scanning the torsion angles allowing the remaining structural parameters to be fully optimised. The minima corresponding to stable conformers and the connecting transition states were also determined. The resulting B3LYP/6-311+G(3df) structures, the derived energy values around the SO–CO bond and the potential energy curve computed with the truncated Fourier series

$$V(\theta) = a_0 + \sum b_n \cos(n\theta) + \sum c_n \sin(n\theta), \qquad (2)$$

as a function of θ, the dihedral angle, are illustrated in Fig. 1. The molecular structures and the electronic potentials corresponding to the OS–OC bond are depicted in Fig. 2. Individual expansion coefficients a_0, b_n and c_n above $n = 3$ do not improve significantly the fits. On the other hand, as there is no guarantee that the individual coefficient values will have real significance, no attempt to explore the transferability assumption of force fields was carried out. Excellent fits of the computed data with squared correlation coefficients r^2 values better than 0.9995 were obtained for both internal rotations.

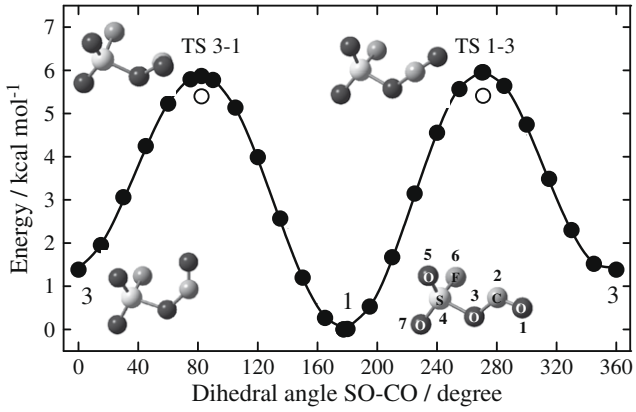

Fig. 1. Potential energy barriers for internal rotation around the SO–CO bond in $FS(O_2)OCO$. (●) B3LYP/6-311+G(3df); (○) G3(MP2)//B3LYP/6-311+G(3df); (—) calculated with Eq. (2) using the coefficients (in kcal mol^{-1}): $a_0 = 3.3142$, $b_1 = 0.7023$, $b_2 = -2.5807$, $b_3 = -8.7170 \times 10^{-3}$, $c_1 = -0.0167$, $c_2 = 0.3294$ and $c_3 = 0.0753$.

Fig. 1 shows that an absolute minimum with a C–O bond *trans*-regarding to O–S bond, and C–O bond *gauche*-regarding to S–F bond is predicted by B3LYP/6-311+G(3df) calculations (conformer 1). This rotamer is 1.4 kcal mol^{-1} more stable than the conformer 3. In addition, two barriers between these minima of about 5.9 kcal mol^{-1} were found. The imaginary vibrational frequencies for the transition states connecting conformers $1 \rightarrow 3$ and $3 \rightarrow 1$ are, respectively, 175i and 181i cm^{-1}. More accurate G3(MP2)//B3LYP/6-311+G(3df) calculations led to a slightly lower barrier of 5.4 kcal mol^{-1}. As Fig. 2 shows, by changing the OS–OC dihedral angle three minima and three maxima are obtained. The two minima with the same lowest energy do not correspond to different conformational isomers but to optical isomers. They are separated by an electronic barrier of 2.8 kcal mol^{-1} at the B3LYP/6-311+G(3df) level and of 3.5 kcal mol^{-1} at the G3(MP2)//B3LYP/6-311+G(3df) level. The other minima correspond to the *trans–trans* conformer (conformer 2). The barriers between the conformers 1 and 2 are 1.1 and 1.3 kcal mol^{-1} at the B3LYP/6-311+G(3df) and G3(MP2)//B3LYP/6-311+G(3df) levels, respectively.

It should be noted that the experimental studies of the $FS(O_2)OF$ and $FS(O_2)OCl$ molecules indicate, as for the $FS(O_2)OCO$, a *gauche* conformation for XOSF (X = F, Cl) as the most stable [27]. In addition, the *trans* conformation for the SO–CO dihedral angle in $FS(O_2)OCO$ is similar to those predicted for the radicals CX_3OCO (X = H [28], F [29]), *trans–trans* respect to XCO–CO.

3.2. Molecular geometry and harmonic vibrational frequencies

The equilibrium structure of the most stable $FS(O_2)OCO$ conformer was determined combining the functionals B3LYP, B98, B97-2, O3LYP, X3LYP, and BMK with the 6-311+G(3df) basis set. The average values for the computed bond lengths and angles with the last four functional, differ in only ±0.02 Å and ±0.6° with those calculated via the B3LYP approach. At the predicted structures, unscaled harmonic vibrational frequencies and infrared intensities were calculated. For the sake of simplicity, only the molecular properties derived at the B3LYP/6-311+G(3df) level are presented here. However, the vibrational frequencies calculated at all mentioned levels of theory were used to estimate the zero-point energies and the thermal corrections to the internal energy (298.15 K, 1 atm) employed in the thermochemical calculations. Table 1 shows the very good agreement obtained in the geometrical

Table 1
Calculated bond lengths (in Å) and angles (in °) for the $FS(O_2)OCO$ and for the transition state $[FS(O_2)O\cdots CO]^{\#}$.

Parameter	$FS(O_2)OCO$[a]	$FS(O_2)OCO$[b]	$[FS(O_2)O\cdots CO]^{\#}$[a]
$r(C_2–O_1)$	1.165	1.166	1.125
$r(C_2–O_3)$	1.385	1.396	1.972
$r(O_3–S_4)$	1.624	1.624	1.543
$r(S_4–O_5)$	1.411	1.417	1.414
$r(S_4–F_6)$	1.563	1.576	1.571
$r(S_4–O_7)$	1.408	1.412	1.425
$\angle(O_1–C_2–O_3)$	124.4	124.6	121.7
$\angle(C_2–O_3–S_4)$	118.3	117.1	116.6
$\angle(O_3–S_4–O_5)$	110.5	110.1	113.9
$\angle(O_3–S_4–F_6)$	97.5	97.2	100.7
$\angle(O_3–S_4–O_7)$	105.1	105.4	104.1
$DIH(O_1–C_2–O_3–S_4)$	177.4	177.2	173.8
$DIH(C_2–O_3–S_4–O_5)$	−38.6	−40.3	−41.4
$DIH(O_5–O_3–S_4–F_6)$	111.7	111.0	113.2
$DIH(O_5–O_3–S_4–O_7)$	−137.4	−138.3	−136.4

[a] B3LYP/6-311+G(3df).
[b] CCSD/6-311G(d).

parameters computed at the B3LYP/6-311+G(3df) and CCSD/311G(d) levels of theory.

In average, the characteristics bond lengths and angles for the $FS(O_2)O$ group in the $FS(O_2)OCO$ differ in only ±0.02 Å and ±2.0° with the values reported for $FS(O_2)OX$ (X = F, Cl) [27], $FS(O_2)OO(O_2)SF$ [30] and $FS(O_2)OCH_3$ [31]. On the other hand, the O–CO bond distances and the O–C=O angles are quite similar in $FS(O_2)OCO$ and CF_3OCO radicals [28].

Table 2
Harmonic vibrational frequencies (in cm^{-1}), approximate assignment and infrared intensities (in $km\,mol^{-1}$) of the $FS(O_2)OCO$ radical and the transition state $[FS(O_2)O\ldots CO]^{\#}$ calculated at the B3LYP/6-311+G(3df) level.

Assignment	$FS(O_2)OCO$	$[FS(O_2)O\cdots CO]^{\#}$
Str C=O	1930 (244)	2188 (165)
Str asym. O=S=O	1497 (244)	1425 (186)
Str sym. O=S=O	1253 (159)	1193 (68)
Str C–O	939 (244)	249i (30)
Str S–O	825 (330)	842 (152)
Str S–F	800 (164)	779 (96)
Wag $FS(O_2)O$	606 (138)	537 (44)
Umbrella $FS(O_2)O$	523 (15)	527 (16)
Rock FSO_2	514 (13)	492 (13)
Wag $FS(O_2)O$	420 (4)	367 (1)
Out of plane SOC	370 (2)	370 (6)
Bend FSO	360 (2)	286 (24)
Out of plane OCO	177 (3)	135 (2)
Torsion SO–CO	158 (4)	50 (0.4)
Torsion OS–OC	78 (0.4)	98 (0.9)[a]

[a] A bend motion instead of a torsion is assigned at the transition state.

Calculated harmonic vibrational frequencies, approximate mode assignment and infrared intensities are listed in Table 2. Mode descriptions were obtained from the animation of the normal modes and by comparison with the spectra of analogous compounds. Certainly, some of the modes are strongly mixed (mainly between 420 and 606 cm^{-1}) and hence, only approximate assignment are given. The vibrational frequencies calculated with the B98, B97-2, O3LYP, X3LYP, and BMK functionals differ with those given in Table 2 in about ±60 cm^{-1}.

3.3. Thermochemistry

In order to determine the thermodynamic stability of $FS(O_2)OCO$, its standard enthalpy of formation at 298 K, $\Delta H_{f,298}$, was calculated. This property was estimated from two well-known methods. Firstly, we calculated the total atomization energy of $FS(O_2)OCO$ into its constituents atoms at 0 K, ΣD_0, with explicit consideration of atomic spin-orbit effects. Then, by subtraction ΣD_0 from the sum of the experimental $\Delta H_{f,0}$ values of each constituent atom [32], and after appropriate corrections by thermal contributions, $\Delta H_{f,298}$ is derived. The second method relies on the calculation of the enthalpy change, ΔH_r, of a selected isodesmic and isogyric reaction. In these reactions, the number of each type of bonds in reactants and products, as well as the spin multiplicities are conserved and, in consequence, systematic errors due to both deficiencies in the treatment of the electron correlation energy and truncation of the basis sets, are reduced by compensations.

The thermochemical data determined by the atomization procedure are listed in Table 3. It can be observed that the $\Delta H_{f,298}$ values derived from the DFT calculations span over a range of about 17 kcal mol^{-1}, while less spreading is predicted by the composite *ab initio* models. The last version of these models, the G4, leads to $\Delta H_{f,298}$ values close to those derived at the B97-2 and BMK levels. In addition, the G4 enthalpies are similar to those predicted at the accurate BAC-G3//B3LYP/6-311+G(3df) level. It should be noted that the atomization method requires an accurate determination of the energy of the molecule and its constituent atoms and, therefore, places stringent requirements on the quantum methods employed. In particular, owing to the presence of lone pair electrons on O atoms, the correlation effects are expected to be here relevant.

To confront with the above $\Delta H_{f,298}$ values we have used the working reaction (3) with its associated enthalpy $\Delta H_{r,3}$

$$HFSO_3 + H_2CO + CH_3OH + CH_3 \rightarrow FS(O_2)OCO + 2CH_4 + H_2O \quad (3)$$

The $\Delta H_{f,298}$ values for $FS(O_2)OCO$ were obtained by combining the computed $\Delta H_{r,3}$ values with reliable enthalpies of formation of the other molecules present in the reaction. To this end, we have used the following well-established enthalpies of formation (in kcal mol^{-1}) from Ref. [33]: −25.98 ± 0.01 for H_2CO, −48.04 ± 0.14

Table 3
Atomization energies, enthalpy changes for the reaction (3) and derived enthalpies of formation (in kcal mol^{-1}) for the $FS(O_2)OCO$ radical.

Level of theory	ΣD_0	$\Delta H_{f,298}$[a]	$\Delta H_{r,3}$	$\Delta H_{f,298}$[b]
B3LYP/6-311++G(3df,3pd)	625.8	−141.2	−28.7	−154.3
B98/6-311++G(3df,3pd)	638.0	−149.7	−28.9	−154.5
B97-2/6-311++G(3df,3pd)	642.6	−154.4	−29.6	−155.2
O3LYP/6-311++G(3df,3pd)	632.7	−144.4	−29.9	−155.5
X3LYP/6-311++G(3df,3pd)	626.8	−138.5	−28.2	−153.8
BMK/6-311++G(3df,3pd)	643.9	−155.9	−29.0	−154.6
G3(MP2)//B3LYP/6-311++G(3df,3pd)	636.8	−148.5	−28.8	−154.4
G3//B3LYP/6-311++G(3df,3pd)	639.1	−150.8	−29.3	−154.8
BAC-G3//B3LYP/6-311++G(3df,3pd)	644.7	−156.4	−31.9	−157.4
G4	643.1	−154.8	−30.3	−155.9
Average values	637.4 ± 7.1	−149.5 ± 6.5	−29.5 ± 1.1	−155.0 ± 1.1

[a] Calculated by atomization.
[b] Calculated using reaction (3).

Please cite this article in press as: M.E. Tucceri et al., Chem. Phys. Lett. (2010), doi:10.1016/j.cplett.2010.03.036

for CH_3OH, 35.05 ± 0.07 for CH_3, −17.80 ± 0.10 for CH_4 and −57.798 ± 0.010 for H_2O. A value of −180.0 ± 2.0 kcal mol^{-1} was employed for $HFSO_3$ [32,34]. The resulting $\Delta H_{r,3}$ and $\Delta H_{f,298}$ values at different levels of theory are presented in Table 3. The quoted error is 3σ. The large scatter observed in the $\Delta H_{f,298}$ values obtained by the atomization method are notably reduced by employing the isodesmic reaction (3). This fact clearly shows that the afore-mentioned systematic compensation of errors is really operative for the present case. In particular, a very good agreement between the $\Delta H_{f,298}$ values calculated from atomization and from isodesmic energies is obtained when the accurate methods BAC-G3//B3LYP/6-311++G(3df,3pd) (average error 0.44 kcal mol^{-1}) [26] and G4 (average error 0.80 kcal mol^{-1}) [25] are employed. The best value obtained averaging all isodesmic data of Table 3 is $\Delta H_{f,298}$ = −155.0 ± 2.0 kcal mol^{-1}. A value of $\Delta H_{f,0}$ = −153.2 ± 2.0 kcal mol^{-1} is obtained at 0 K after correction by DFT thermal contributions. The assigned conservative error limit of ±2.0 kcal mol^{-1} is larger than that given in Table 3, and results from the uncertainty in the enthalpy of formation of $HFSO_3$ [32,34].

3.4. Kinetics of the reaction $FSO_3 + CO \rightarrow FS(O_2)OCO$

In a previous study, we have employed the laser flash photolysis technique to investigate the recombination reaction of FSO_3 radicals with FCO_2 radicals and with CO [9]. For the last reaction, a high pressure rate coefficient of $k_{1,\infty} = (4.3 \pm 0.9) \times 10^{-17}$ cm^3 molecule^{-1} s^{-1} was determined at 296 K. This small value indicated that in the association of the FSO_3 radical with CO an electronic energy barrier is present. In fact, the essential features of this activated process were outlined in a preliminary DFT study [9]. A more detailed theoretical study of the kinetics of reaction (1) is here reported. The geometries, vibrational frequencies and total energies of the reactants, products and the connecting transitions states were determined with the B3LYP, B98, B97-2, O3LYP, X3LYP and BMK hybrid functional in combination with the 6-311+G(3df) basis set. In addition, more accurate Gaussian-3 and Gaussian-4 calculations were carried out. A standard normal-mode-analysis indicates that all obtained transition state structures led to only one imaginary frequency indicating the presence of true transitions states. In particular, the geometrical parameters and the vibrational frequencies of the transition state $[FS(O_2)O\cdots CO]^{\#}$ computed at the B3LYP/6-311+G(3df) level are presented in Tables 1 and 2. The computed electronic barriers $\Delta H^{\circ\#}_{1,0}$, and enthalpy changes for reaction (1), ΔH°_1, at the different quantum-chemical levels are listed in Table 4. It can be observed that the reaction is exothermic in 3.0–7.7 kcal mol^{-1}. A more accurate enthalpy change of $\Delta H^{\circ}_1 = -6.7$ kcal mol^{-1} can be obtained using our best value for $FS(O_2)OCO$ of $\Delta H_{f,0} = -153.2$ kcal mol^{-1} and enthalpy of formation values of −119.3 and −27.2 kcal mol^{-1} for FSO_3 [9] and CO [32].

The calculations predict a transition state located at about 5.6–8.6 kcal mol^{-1} above the reactants. Most of the DFT calculations together with the Gaussian-3 methods lead to electronic barrier values in very good agreement with the value $\Delta H^{\circ\#}_{1,0} = E_1 - 2RT = 6 \pm 1$ kcal mol^{-1} derived from the experimental activation energy of $E_1 = 7 \pm 1$ kcal mol^{-1} [2]. In fact, the average $\Delta H^{\circ\#}_{1,0}$ value is 6.4 ± 1.0 kcal mol^{-1}. It should be noted that the BMK functional (Boese–Martin for kinetics) [22], especially developed for thermochemical kinetics, predicts ΔH°_1 and $\Delta H^{\circ\#}_{1,0}$ values very close to the best results.

To calculate the rate coefficient of reaction (1), k_1, the microscopic formulation of the transition state theory was employed. For this, the vibrational and rotational partition functions were calculated using the molecular input data obtained from the DFT and *ab initio* calculations. Due to the weakness of the $FS(O_2)O$–CO bond in the transition state, the equilibrium torsional frequency of 158 cm^{-1} is reduced to 50 cm^{-1} at the critical configuration. Hence, taking into account that the torsional frequency and the barrier height are directly related [35,36], a value for the energy barrier much smaller than the equilibrium of 5.4 kcal mol^{-1} is expected at the transition state configuration. Under these conditions, the rotation around the SO–CO bond was assumed free (moment of inertia of I_m = 57.7 amu Å^2). Therefore, a smooth evolution between rotational states of the FSO_3 and CO molecules passing for a $FS(O_2)O$–CO free-rotor transition state to rovibrational excited $FS(O_2)OCO$ adducts is expected along the recombination path. Afterwards, a complex interplay between collisional and intramolecular (unimolecular) processes lead to thermalized populations of the different rotamers. According to Section 3.1, the Botzmann population of rotamer 1 is about ten times larger than the corresponding to rotamer 3 at room temperature. Fig. 3 shows the energy diagram for the potential energy surface of the system, that is, total energy plus zero-point energy corrections.

The resulting preexponential factors A_1 together with the $\Delta H^{\circ\#}_{1,0}$ obtained by its comparison with the experimental $k_{1,\infty} = 4.3 \times 10^{-17}$ cm^3 molecule^{-1} s^{-1} [9] are given in Table 4. As can be appreciated, all A_1 values are spread within a factor of three, being the average value of $(9.7 \pm 4.5) \times 10^{-13}$ cm^3 molecule^{-1} s^{-1}. On the other hand, the derived average value of $\Delta H^{\circ\#}_0 = 5.9 \pm 0.3$ kcal mol^{-1} is in very good agreement with the obtained from the experiments of 6 ± 1 kcal mol^{-1} [2] and from direct calculations of

Table 4
Electronic energy barriers, reaction enthalpies at 0 K (in kcal mol^{-1}), preexponential factors and rate coefficients (in cm^3 molecule^{-1} s^{-1}) for the reaction $FS(O_2)O + CO \rightarrow FS(O_2)OCO$ at 296 K.

Level of theory	$FS(O_2)O + CO \rightarrow [FS(O_2)O\cdots CO]^{\#}$			$FS(O_2)O + CO \rightarrow FS(O_2)OCO$	k_1
	$\Delta H^{\circ\#}_{1.0}$	A_1	$\Delta H^{\circ\#}_{1.0}$ [a]	ΔH°_1	
B3LYP/6-311+G(3df)	6.27	9.65×10^{-13}	5.89	−3.88	2.3×10^{-17}
B98/6-311+G(3df)	5.78	8.38×10^{-13}	5.81	−5.33	4.5×10^{-17}
B97-2/6-311+G(3df)	6.43	8.54×10^{-13}	5.82	−5.83	1.5×10^{-17}
O3LYP/6-311+G(3df)	8.63	1.35×10^{-12}	6.09	−2.97	5.8×10^{-19}
X3LYP/6-311+G(3df)	5.66	7.48×10^{-13}	5.74	−4.90	4.9×10^{-17}
BMK/6-311+G(3df)	5.69	1.47×10^{-12}	6.14	−7.66	9.2×10^{-17}
G3(MP2)//B3LYP/6-311+G(3df)	5.58	9.65×10^{-13}	5.89	−7.38	7.3×10^{-17}
G3//B3LYP/6-311+G(3df)	5.82	9.65×10^{-13}	5.89	−7.31	4.9×10^{-17}
BAC-G3//B3LYP/6-311+G(3df)	6.59	9.65×10^{-13}	5.89	−6.95	1.3×10^{-17}
G4	7.76	5.93×10^{-13}	5.61	−6.49	1.1×10^{-18}
Average values	6.4 ± 1.0	$(9.7 \pm 4.5) \times 10^{-13}$	5.9 ± 0.3	−5.9 ± 1.6	$(3.6 \pm 3.2) \times 10^{-17}$
Experimental values	6 ± 1 [b]	–	–	–	$(4.3 \pm 0.9) \times 10^{-17}$ [c]

[a] Derived from the calculated A_1 values and $k_1 = 4.3 \times 10^{-17}$ cm^3 molecule^{-1} s^{-1} [9].
[b] Ref. [2].
[c] Ref. [9].

Please cite this article in press as: M.E. Tucceri et al., Chem. Phys. Lett. (2010), doi:10.1016/j.cplett.2010.03.036

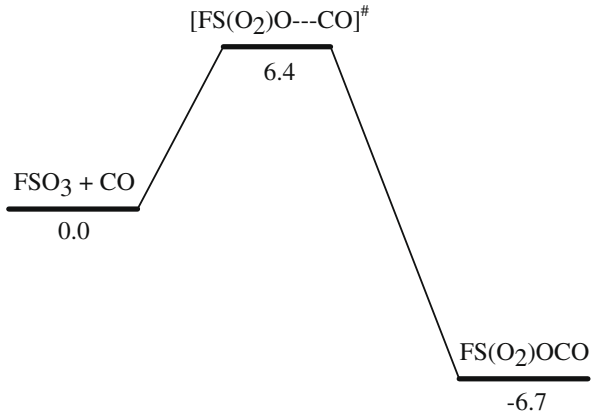

Fig. 3. Schematic diagram of the potential energy surface (in kcal mol^{-1}) for the reaction $FSO_3 + CO \rightarrow FS(O_2)OCO$.

6.4 ± 1.0 kcal mol^{-1}. Table 4 also shows the computed rate coefficients, the average value of $(3.6 \pm 3.2) \times 10^{-17}$ cm^3 molecule^{-1} s^{-1} agrees reasonably with the experimental.

Although a direct experimental observation of $FS(O_2)OCO$ in matrix-isolation conditions is clearly required, the significant electronic barrier of the association process probably difficults its study. However, successful experiments for the determination of the related radical CF_3OCO formed in the three-orders of magnitude faster reaction $CF_3O + CO \rightarrow CF_3OCO$ [33] have been reported [28].

In the indirect studies of Ref. [3] and in the laser flash photolysis experiments of Ref. [9], large O_2 pressures were present. Therefore, the fast association reaction $FS(O_2)OCO + O_2 \rightarrow FS(O_2)OC(O)O_2$ is expected to be dominant under those conditions. The absence of an activation barrier (at the B3LYP/6-311+G(3df) level) supports this conclusion. By contrast, the mechanism was investigated up to reaction times close to 30 min, and under O_2 free conditions in Ref. [2]. The stable product $FS(O_2)O(O_2)SF$ is formed according to $FSO_3 + FSO_2 \rightarrow FS(O_2)O(O_2)SF$ [10]. The FSO_2 radical is generated by the reaction $(FSO_3{\cdot}CO)' \rightarrow FSO_2 + CO_2$, where, according to the original denomination, $(FSO_3{\cdot}CO)'$ is an unidentified excited species formed without activation from $FS(O_2)OCO$. Assuming a similar amount of energy for both species, the activation energy of 16.2 kcal mol^{-1} measured for this dissociative channel [2] compares very well with our G4 estimates for the electronic barrier of 17.1 kcal mol^{-1}. On the other hand, the $(FSO_3{\cdot}CO)'$ species can competitively react with CO regenerating the FSO_3 radical, $(FSO_3{\cdot}CO)' + CO \rightarrow FSO_3 + 2CO$ [2] with an activation energy of 8.5 kcal mol^{-1} [2]. For comparison, a transition state located 7.6 kcal mol^{-1} above the reactants is predicted at the G3(MP2)//B3LYP/6-311++G(3df) level of calculation.

In summary, the present quantum-chemical study has provided new molecular properties for the $FS(O_2)OCO$ radical and allowed to understand, at a molecular level, relevant kinetic features of this species investigated in early and recent experiments from our laboratory.

Acknowledgements

This research project was supported by the Universidad Nacional de La Plata, the Consejo Nacional de Investigaciones Científicas y Técnicas (CONICET), the Agencia Nacional de Promoción Científica y Tecnológica and the Max Planck Institute for Biophysical Chemistry Göttingen through the 'Partner Group for Chlorofluorocarbons in the Atmosphere'.

References

[1] E. Castellano, R. Gatti, J.E. Sicre, H.J. Schumacher, Z. Physik. Chem. NF 42 (1964) 174.
[2] R. Gatti, J.E. Sicre, H.J. Schumacher, Z. Physik. Chem. NF 47 (1965) 323.
[3] R. Gatti, H.J. Schumacher, Z. Physik. Chem. NF 55 (1967) 148.
[4] A.E. Croce de Cobos, C.J. Cobos, E. Castellano, J. Phys. Chem. 93 (1989) 274.
[5] C.J. Cobos, A.E. Croce de Cobos, H. Hippler, E. Castellano, J. Phys. Chem. 93 (1989) 3089.
[6] A.E. Croce, C.J. Cobos, E. Castellano, Chem. Phys. Lett. 158 (1989) 157.
[7] C.J. Cobos, A.E. Croce, E. Castellano, Int. J. Chem. Kinet. 22 (1990) 289.
[8] M.E. Tucceri, M.P. Badenes, A.E. Croce, C.J. Cobos, Chem. Commun. (2001) 71.
[9] M.E. Tucceri, M.P. Badenes, A.E. Croce, C.J. Cobos, Phys. Chem. Chem. Phys. 3 (2001) 1832.
[10] M.E. Tucceri, A.E. Croce, C.J. Cobos, Chem. Phys. Lett. 404 (2005) 232.
[11] G.W. King, C.H. Warren, J. Mol. Spectrosc. 32 (1969) 138 (and references therein).
[12] H. Beckers, H. Willner, D. Grote, W. Sander, J. Chem. Phys. 128 (2008) 84501.
[13] L. Kolesniková, J. Varga, L. Nová Stříteská, H. Beckers, H. Willner, F. Aubke, S. Urban, J. Chem. Phys. 130 (2009) 184309.
[14] Z. Li, Chem. Phys. Lett. 269 (1997) 128.
[15] A.D. Becke, Phys. Rev. A 38 (1988) 3098.
[16] C. Lee, W. Yang, R.G. Parr, Phys. Rev. B 37 (1988) 785.
[17] C. Adamo, V. Barone, J. Chem. Phys. 108 (1998) 664.
[18] F.A. Hamprecht, A.J. Cohen, D.J. Tozer, N.C. Handy, J. Chem. Phys. 109 (1998) 6264.
[19] P.J. Wilson, T.J. Bradley, D.J. Tozer, J. Chem. Phys. 115 (2001) 9233.
[20] W.-H. Hoe, A.J. Cohen, N.C. Handy, Chem. Phys. Lett. 341 (2001) 319.
[21] X. Xu, W.A. Goddard III, Proc. Natl. Acad. Sci. USA 101 (2004) 2673.
[22] A.D. Boese, J.M.L. Martin, J. Chem. Phys. 121 (2004) 3405.
[23] M.J. Frisch et al., Gaussian 03, Revision D.01, Gaussian Inc., Wallingford, CT, 2004.
[24] A.G. Baboul, L.A. Curtiss, P.C. Redfern, K. Raghavachari, J. Chem. Phys. 110 (1999) 7650.
[25] L.A. Curtiss, P.C. Redfern, K. Raghavachari, J. Chem. Phys. 126 (2007) 84108.
[26] B. Anantharaman, C.F. Melius, J. Phys. Chem. A 109 (2005) 1734.
[27] F. Aubke, B. Casper, H.S.P. Müller, H. Oberhammer, H. Willner, J. Mol. Struct. 346 (1995) 111.
[28] S. von Ahsen, J. Hufen, H. Willner, J.S. Francisco, Chem. Eur. J. 8 (2002) 1189.
[29] J.S. Francisco, Chem. Phys. 237 (1998) 1.
[30] K. Hagen, K. Hedberg, G. Gard, F. Aubke, J. Mol. Struct. 567 (2001) 1.
[31] I. Hargittai, R. Seip, K.P. Nair, C.O. Britt, J.E. Boggs, B.N. Cyvin, J. Mol. Struct. 39 (1977) 1.
[32] M.W. Chase Jr., NIST-JANAF Thermochemical Tables, fourth edn., J. Phys. Chem. Ref. Data, 1998, p. 579 (Monograph No. 9).
[33] S.P. Sander et al., Chemical Kinetics and Photochemical Data for Use in Atmospheric Studies, NASA/JPL Data Evaluation, JPL Publication 06-2 Evaluation No. 15, NASA, Pasadena, CA, November 20, 2006.
[34] S.W. Benson, Chem. Rev. 78 (1978) 23.
[35] J. Troe, J. Chem. Phys. 66 (1977) 4758.
[36] J. Troe, J. Phys. Chem. 90 (1986) 3485.